1 # Metazoan zooplankton in the Bay of Biscay: 16 years of
2 # individual sizes and abundances from the ZooScan and
3 # ZooCAM imaging systems.

5 **Authors**

6 Grandremy Nina[1]*, Bourriau Paul[1], Daché Edwin[2], Danielou Marie-Madeleine[3], Doray Mathieu[1], Dupuy
7 Christine[4], Forest Bertrand[5], Jalabert Laetitia[6], Huret Martin[7], Le Mestre Sophie[7], Nowaczyk Antoine[8], Petitgas
8 Pierre[9], Pineau Philippe[4], Rouxel Justin[10], Tardivel Morgan[10], Romagnan Jean-Baptiste[1]*.

9 **Correspondence**

10 grandremy.n@gmail.com, jean.baptiste.romagnan@ifremer.fr

11 **Affiliations**

12 [1] DECOD (Ecosystem Dynamics and Sustainability), IFREMER, INRAE, Institut Agro, Nantes, Centre Atlantique
13 - Rue de l'Ile d'Yeu - BP 21105 - 44311 Nantes Cedex 03, France.

14 [2] Unité Biologie et Ecologie des Ecosystèmes marins Profonds, Laboratoire Environnement Profond, Ifremer
15 Centre Bretagne - ZI de la Pointe du Diable - CS 10070 - 29280 Plouzané, France.

16 [3] Unité DYNECO-PELAGOS, Laboratoire d'Ecologie Pélagique, Ifremer Centre Bretagne - ZI de la Pointe du
17 Diable - CS 10070 - 29280 Plouzané, France.

18 [4] BIOFEEL, UMRi LIENSs, La Rochelle University / CNRS, 2, rue Olympe de Gouges, 17000 La Rochelle,
19 France.

20 [5] Laboratoire Hydrodynamique Marine, Unité RDT, Ifremer Centre Bretagne - ZI de la Pointe du Diable - CS
21 10070 - 29280 Plouzané, France.

22 [6] Sorbonne Université, Institut de la Mer de Villefranche, 06230 Villefranche-sur-mer, France.

23 [7] DECOD (Ecosystem Dynamics and Sustainability), IFREMER, INRAE, Institut Agro, Centre Bretagne - ZI de
24 la Pointe du Diable - CS 10070 - 29280 Plouzané, France.

25 [8] UMR CNRS 5805 EPOC – OASU, Station Marine d'Arcachon, Université de Bordeaux, 2 Rue du Professeur
26 Jolyet, 33120 Arcachon, France.

27 [9] Departement Ressources Biologiques et Environnement, Ifremer Centre Atlantique - Rue de l'Ile d'Yeu - BP
28 21105 - 44311 Nantes Cedex 03, France.

29 [10] Laboratoire Détection, Capteurs et Mesures, Unité RDT, Ifremer Centre Bretagne - ZI de la Pointe du Diable -
30 CS 10070 - 29280 Plouzané, France.

31 * These authors contributed equally to this work.

Abstract

This paper presents two metazoan zooplankton datasets obtained by imaging samples collected on the Bay of Biscay continental shelf in spring during the PELGAS integrated surveys, over the 2004-2019 period. The samples were collected at night, with a WP2 200 µm mesh size fitted with a Hydrobios (back-run stop) mechanical flowmeter, hauled vertically from the sea floor to the surface with a maximum depth set at 100 m when the bathymetry is deeper. The first dataset originates from samples collected from 2004 to 2016, imaged on land with the ZooScan and is composed of 1,153,507 imaged and measured objects. The second dataset originates from samples collected from 2016 to 2019, imaged on board the R/V *Thalassa* with the ZooCAM and is composed of 702,111 imaged and measured objects. The imaged objects is composed of zooplankton individuals, zooplankton pieces, non-living particles and imaging artefacts, ranging from 300 µm to 3.39 mm Equivalent Spherical Diameter, individually imaged, measured and identified. Each imaged object is geolocated, associated to a station, a survey, a year and other metadata. Each object is described by a set of morphological and grey level based features (8 bits encoding, 0 = black, 255 = white), including size, automatically extracted on each individual image. Each object was taxonomically identified using the web based application Ecotaxa with built-in, random forest and CNN based, semi-automatic sorting tools followed by expert validation or correction. The objects were sorted in 172 taxonomic and morphological groups. Each dataset features a table combining metadata and data, at the individual object granularity, from which one can easily derive quantitative population and communities descriptors such as abundances, mean sizes, biovolumes, biomasses, and size structure. Each object's individual image is provided along with the data. These two datasets can be used combined together for ecological studies as the two instruments are interoperable, or as training sets for ZooScan and ZooCAM users.

Keywords

Zooplankton, ZooCAM, ZooScan, Bay of Biscay, imaging, PELGAS surveys.
1 Introduction

Metazoan heterotrophic planktonic organisms, hereafter referred to as zooplankton, encompass an immense diversity of life forms, which have successfully colonized the entire ocean, from eutrophic estuarine shallow areas to oligotrophic open ocean, from sunlit ocean to hadal depth. Their body sizes span five to six orders of magnitude in length, from µm to tens of meters (Sieburth & Smetacek, 1978). Zooplankton plays a pivotal role in marine ecosystem (Banse, 1995). It transfers the organic matter produced in the epipelagic domain by photosynthesis to the deeper layers of the ocean (Siegel et al., 2016), by producing fast sinking aggregates (Turner, 2015), and by diel vertical migration (Steinberg et al., 2000; Ohman & Romagnan, 2016). Zooplankton therefore participates in mitigating the anthropogenic carbon dioxide build up in the atmosphere responsible for climate change. Moreover, zooplankton is an exclusive trophic resource for commercially important fish during their larval stage, where a shift in zooplankton species or phenology can have dramatic effects on recruitment (i.e. North Sea cod, Beaugrand et al., 2003). In addition, it is a major trophic resource for adult planktivorous small pelagic fish, known as forage fishes (Van der Lingen, 2006). Recent studies suggest that zooplankton dynamics may have a significant effect on small pelagic fish population dynamics and individual body condition (Brosset et al., 2016; Menu et al., 2023), and therefore impact wasp-waist ecosystem based fisheries and fisheries dependent socio-ecosystems, worldwide (Cury et al., 2000).

Despite zooplankton being of such global importance in both climate change effects on ecosystems and management of fisheries (Chiba et al., 2018; Lombard et al., 2019), it is still technically difficult to monitor, with respect to other marine ecological compartments. Zooplankton biomass, diversity and spatio-temporal distributions cannot be estimated from spaceborne sensors as phytoplankton's does (Uitz et al., 2010), and zooplankton commercial exploitation data do not exist yet, as fish data does. One noticeable exception is the CPR surveys network that enables zooplankton data generation at decent spatio-temporal scales (Batten et al., 2019). Yet, generating zooplankton data often requires dedicated surveys at sea, specific sampling instruments and trained analysts. Moreover, besides actual observation, modelling zooplankton remains a challenging task due to the diversity of traits such as life forms, life cycles, body sizes and physiological processes exhibited by zooplankton (Mitra & Davis 2010; Mitra et al., 2014). However, over the past two decades the development of imaging and associated machine learning semi-automatic identification tools (Irisson et al., 2022) have greatly improved the capability of scientists to analyse long (Feuilloley et al., 2022), high frequency (Romagnan et al., 2016), or spatially resolved (Grandremy et al., 2023a) zooplankton time series, as well as trait based data (Orenstein et al., 2022). Imaging and machine learning have particularly enabled the increased development of combined size and taxonomy zooplankton ecological studies (i.e. Vandromme et al., 2014; Romagnan et al., 2016; Benedetti et al., 2019). Yet, use of these machine learning tools is not trivial because those often require abundant, scientifically qualified, sensor specific, training image data (i.e. learning set and test set, Irisson et al., 2022), and complex hardware and software setups (Panaïotis et al., 2022). One good example of such image dataset is the ZooScanNet dataset (Elineau et al., 2018), which features an extensive ZooScan (Gorsky et al., 2010) imaging dataset usable as a training set for ecologists as well as for imaging and machine learning scientists.

The objective of this paper is to present two open zooplankton imaging datasets, originating from two different instruments, the ZooScan (Gorsky et al., 2010), and the ZooCAM (Colas et al., 2018). These datasets originate from the PELGAS integrated survey in the Bay of Biscay (Doray et al., 2018), a continental shelf

94 ecosystem supporting major European fisheries (ICES, 2021). Combined together, these datasets make up a 16
95 years time series of sized and taxonomically resolved zooplankton, along with context metadata allowing the
96 calculation of quantitative data, covering the whole Bay of Biscay continental shelf, from the French coast to the
97 continental slope, and from the Basque country to southern Brittany, in spring. These datasets can be used for
98 ecological studies (Grandremy et al., 2023a), machine learning studies, and modelling studies.

2 Methods

2.1 Sampling

101 Zooplankton samples were collected during the successive PELGAS integrated surveys (Doray et al.,
102 2018) carried out over the Bay of Biscay French continental shelf, in spring from 2004 to 2019 on board the R/V
103 *Thalassa*. The number of samples across years varied between 41 (2005) and 64 (2019), due to adjustments in the
104 sampling strategy and weather conditions, for 889 zooplankton samples collected in total. From 2004 to 2006,
105 samples were collected in the southern Bay of Biscay until the Loire estuary only (Fig. 1). Sampling was carried
106 out in vertical tows during night time using a 200-µm mesh size WP2 net, generally from 100 m depth (or 5 m
107 above the seabed) to the surface. In 2004 and 2005, the targeted maximum sampling depth was 200 m. In 2004,
108 fifteen samples were collected deeper than 100 m, among which eleven were deeper than 120 m; in 2005, twenty
109 samples were collected deeper than 100 m, among which thirteen were deeper than 120 m. Before 2014, the
110 sampled water volume was estimated by multiplying the cable length by the net opening surface (0.25 m²) whereas
111 since 2014, the net was equipped with a Hydrobios back-run stop flowmeter. The samples originating from 2004
112 to 2016 surveys were preserved in 4% formaldehyde (final concentration) and analysed on land in the laboratory
113 with the ZooScan in 2019, while since 2016 they were analysed live on board with the ZooCAM.

2.2 Sample processing and analyses

2.2.1 Digitization with the ZooScan

116 Preserved samples were digitized with the ZooScan (Gorsky et al., 2010), a flatbed scanner generating
117 16-bit gray-level high-resolution images (2400 dpi, pixel size: 10.56 µm, image size: 15×24 cm equivalent to
118 14 200×22 700 pixels). It is well suited for the imaging of preserved organisms ranging in size from 300 µm to
119 several centimeters. The ZooScan is run by the custom made, ImageJ based, ZooProcess software which generates
120 one single large image for each scan that contains up to 2000 organisms depending on the size of the imaged
121 organisms.

122 Prior to digitization, the seawater and formaldehyde solution was filtered through a 180 µm mesh sieve
123 into a trash tank, under a fume hood. The organisms were then gently but thoroughly rinsed with freshwater over
124 the tank, in the sieve. They were then size-fractionated with a 1 mm sieve, into organisms larger and smaller than
125 1 mm size fractions. This size splitting step is recommended when using the ZooScan to address the possible
126 under-representation of large objects bias caused by the necessary subsampling. Each size fraction was subsampled
127 separately with a Motoda splitter to obtain two subsamples containing 500-1000 objects for the large organisms
128 size fraction, and 1000-2000 objects for the small organisms size fraction. Each subsample was imaged after
129 manual separation of objects on the scanning tray, to mitigate the number of overlapping objects as recommended
130 in Vandromme et al., 2012. Overall, 699 samples were digitized following this protocol, corresponding to 1397
131 scans (one sample was not size fractioned as it did not contained organisms larger than 1 mm).

132
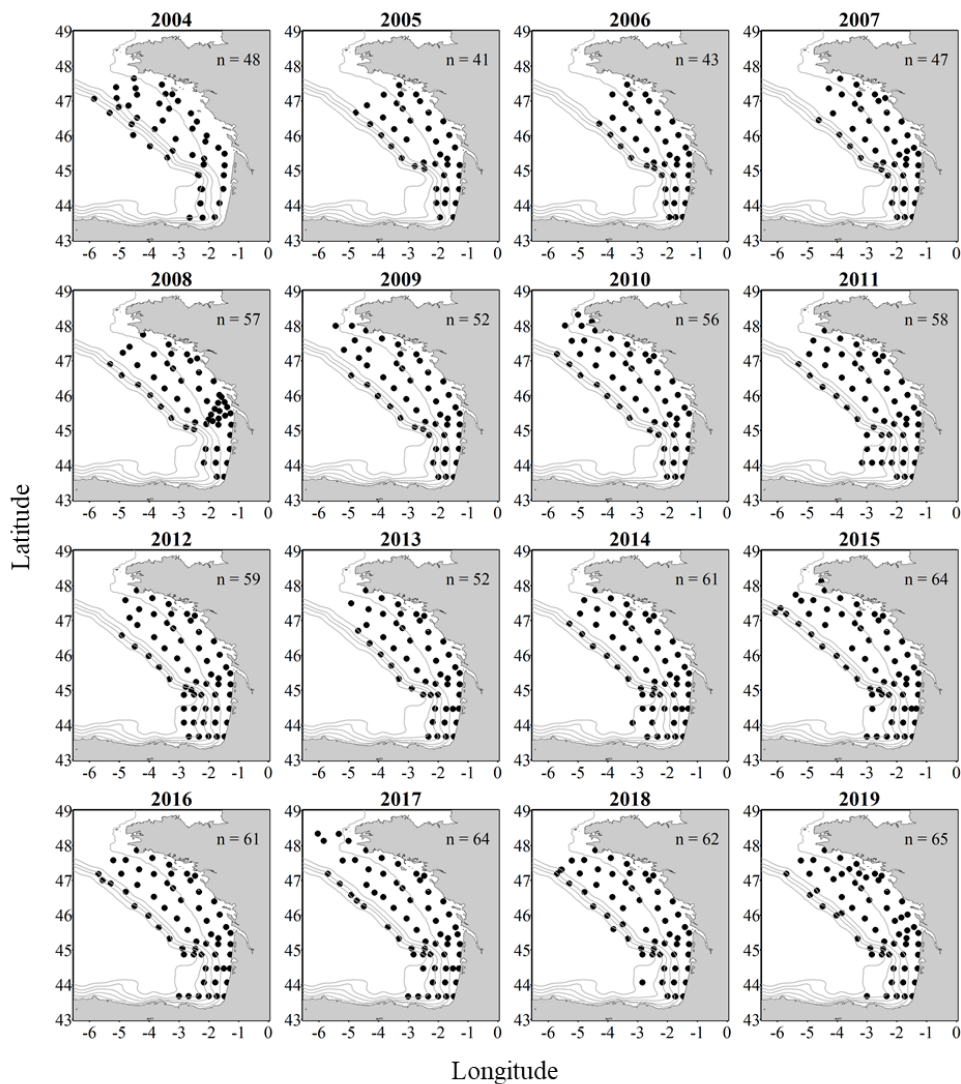
Figure 1: Metazoan zooplankton sampling locations during the PELGAS cruises in the Bay of Biscay from 2004
to 2019. The years with the poorest coverage are 2005 and 2006 with 41 and 43 sampling stations respectively;
and the years with the best coverage are 2015, 2017 and 2019 with 64, 64 and 65 sampling stations respectively.

2.2.2 Digitization with the ZooCAM

The ZooCAM is an in-flow imaging instrument, designed to digitize preserved as well as live zooplankton samples, on board, immediately after collection (Colas et al., 2018). The ZooCAM features a cylindrical transparent tank in which the zooplankton sample is mixed with filtered seawater. Depending on the richness of the sample, and the subsampling (if necessary), the volume of seawater can be adjusted between 2-7 litres. The organisms were pumped at a 1L.min^{-1} from the tank to a flowcell inserted between a CCD camera (pixel size: 10.3 µm) and a red LED flashing device where they were imaged at 16 fps. Given the flowcell volume, the size of the field of view, the imaging frequency and the flowrate, all the seawater volume containing the organisms was imaged (Colas et al., 2018). Before all the initial volume was imaged, the tank and the tubing were carefully and thoroughly rinsed with filtered seawater to ensure the imaging of all the organisms poured in the tank. For each sample, the ZooCAM generates a stack of small size (~1 Mo) raw images that are subsequently analysed with the ZooCAM software. Depending on the initial water content of the tank and the rinsing, a ZooCAM run can generate up to 10k raw images from which the individual organism vignettes will be extracted. A ZooCAM run on a live sample often generates up to 5000-10000 vignettes of individual organisms. It is very important to subsample the initial samples with a dichotomic splitter (here a Motoda splitter), to get subsamples with a quantity of objects that reduce the risk of imaging overlapping objects, and to break free from the dependency to the water volume imaged to reconstruct quantitative estimates of zooplankton as the initial and rinsing volume are variable. Overall, 190 samples were digitized live on-board with the ZooCAM.

2.3 Images processing

Both instruments generate grey level working images (8 bit encoding, 0 = black, 255 = white). In both cases, image processing consisted in (i) a "physical" background homogenization by subtracting an empty background image to each sample image (1 for ZooScan, and as many as raw images for ZooCAM), (ii) a thresholding of each raw image (threshold value: 243 for ZooScan, 240 for ZooCAM), (iii) the segmentation of each object imaged. The ZooProcess software was set to detect and segment objects with an area equal or larger than 631 pixels, whereas the ZooCAM software was set to detect objects with an area equal or larger than 667 pixels, which in both cases equals 300 µm ESD, or a biovolume of 0.014 mm^3 (using a spherical biovolume model, Vandromme et al., 2012).

Morphological features were then extracted on each detected object. Features generated by the ZooScan are defined in Gorsky et al. (2010) and those generated by the ZooCAM are defined in Colas et al. (2018). ZooScan images were processed with ZooProcess v7.39 (04/10/2020) open source software. ZooCAM images were processed with the proprietary ZooCAM custom made software which uses the MIL (Matrox Imaging Library, Dorval, Québec, Canada) as the individual object processing kernel. Each detected object was finally cropped from the working sample images, and saved as a unique, labelled vignette, in a sample specific folder along with a sample specific single text file containing the objects features arranged as a table with objects arranged in lines and features in columns.

2.4 Touching objects

The ZooProcess features a tool that enable the digital separation of possible touching objects in the final image dataset, for each sample. As touching objects may impair the estimations of abundances and size structure

174 (Vandromme et al., 2012), remaining touching objects were searched for on the individual vignettes from the
175 ZooScan and digitally manually separated with the ZooProcess separation tool to improve the quality of further
176 identifications, counts and size structure of zooplankton. ZooCAM does not offer such a tool.

2.5 Taxonomic identification of individual images

178 All individual vignettes from both instruments were sorted and identified with the help of the online
179 application Ecotaxa (Picheral et al., 2017), as two instrument-specific separated sets. Ecotaxa features a Random
180 Forest algorithm (Breiman, 2001) and a series of instruments specific tuned spatially sparse Convolutional Neural
181 Networks (Graham, 2014) that were used in a combined approach to predict identifications of unidentified objects.
182 First, an automatic classification of non-identified individual vignettes into coarse zooplankton and non-
183 zooplankton categories was carried out. In both cases (ZooScan and ZooCAM), Ecotaxa hosted instrument specific
184 image datasets, previously curated and freely available, were used as initial learning sets. These initial
185 classifications were then visually inspected, manually validated or corrected when necessary, and taxonomically
186 refined when possible. After a few thousand images were validated in each project, they were used as dataset
187 specific learning sets to improve the initial coarse automatic identifications. This process was iterated until all the
188 individual vignettes were classified into their maximum reachable taxonomical detail. It is worth mentioning here
189 that only a handful of taxonomists worked on identification of the two images sets.

2.6 Intercalibration of the two instruments

191 The two datasets are usable separately. However, considered together they build a 16 years long spatio-
192 temporal time series. To ensure they are homogeneous and can thus be used together for ecological studies, we
193 conducted a comparison study using samples from year 2016 (61 stations over the whole Bay of Biscay continental
194 shelf, Grandremy et al., under review). In brief, all non-zooplankton and touching objects images were removed
195 from the initial datasets. Then, the interoperable size range was determined with an assessment based on the
196 comparison of Normalized Biovolume – Size Spectra (NB-SS) for each instrument. This size interval ranges
197 between [0.3-3.39] mm ESD. Finally, the zooplankton communities as seen by the ZooScan and the ZooCAM
198 were compared by taxa and by station using 27 taxonomic groups. Poorly represented taxa as well as non-
199 taxonomically identified objects were not taken into account in the zooplankton variables computation and in
200 community structure analyses. Both instruments showed similar NB-SS slopes for 58 out of 61 stations; depicted
201 comparable abundances, biovolumes and mean organisms' sizes, as well as similar community composition for a
202 majority of sampling stations. They also estimated similar spatial patterns of the zooplankton community at the
203 scale of the Bay of Biscay. We therefore assume that the two presented datasets build a single, 16 years long spatio-
204 temporal time series of abundances (Fig. 2) and sizes of zooplanktonic organisms (Fig. 3), from which biovolumes,
205 biomasses, Shannon index (Fig. 4), and zooplankton community size structure can be derived (Vandromme et al.,
206 2012).
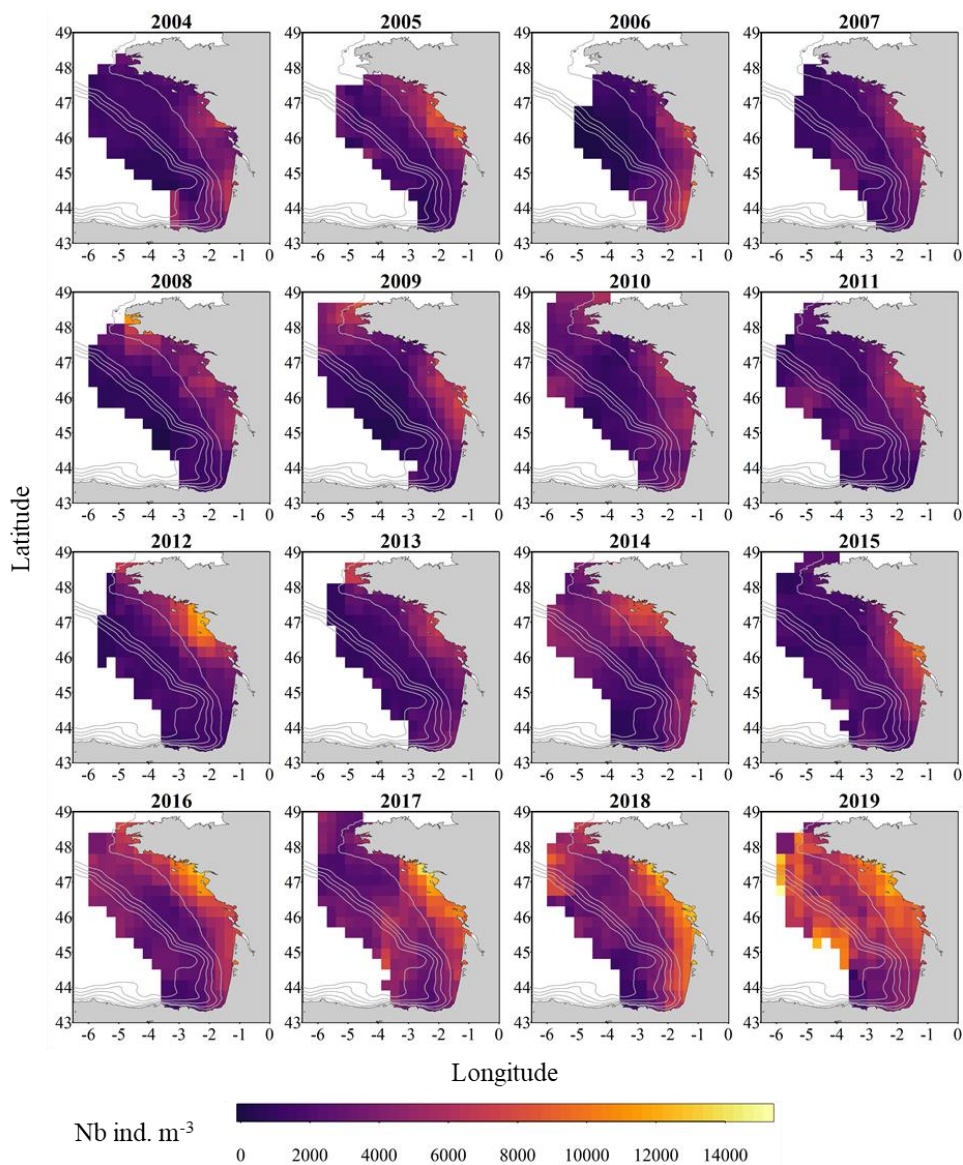
Figure 2: Gridded maps of total zooplankton abundances expressed as individuals per cubic meters of sampled seawater, during the PELGAS cruises in the Bay of Biscay from 2004 to 2019. The abundances are well within the range of zooplankton abundances seen over other temperate continental shelves. They exhibit a marked coastal to offshore gradient, abundances being higher at the coast. Abundances also show an overall increase over the years.
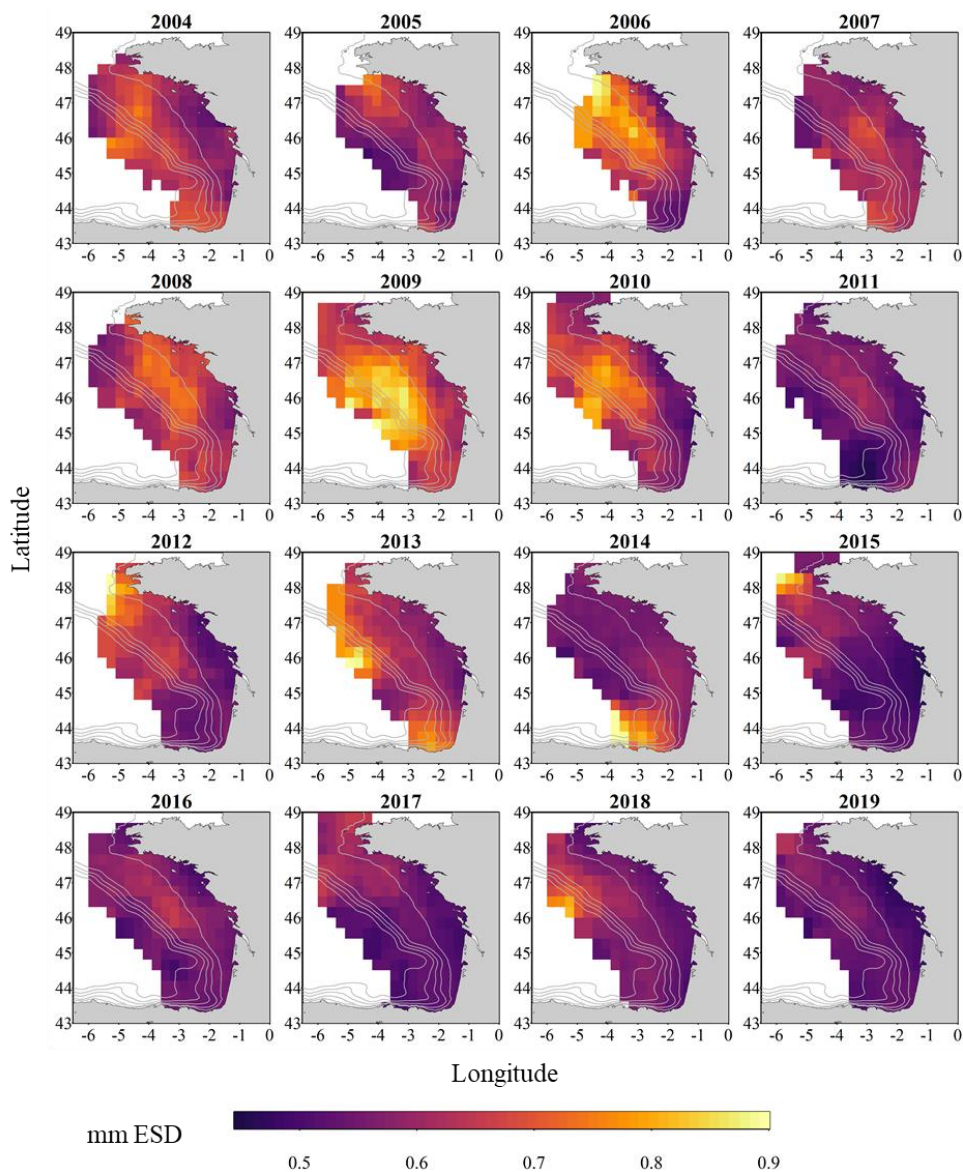
Figure 3: Gridded maps of total zooplankton mean sizes expressed as mm Equivalent Spherical Diameter during the PELGAS cruise in the Bay of Biscay from 2004 to 2019. They exhibit a coastal to offshore gradient as well as a north-south gradient. Mean body sizes are smaller at the coast and usually smaller in the south. In general, mean body sizes show an overall decrease over the years.

3 Datasets

3.1 Taxonomic groups and Operational Taxonomic Units

The ZooScan dataset is composed of 1,153,507 zooplankton individuals, zooplankton parts, non-living particles and imaging artefacts individually imaged and measured with the ZooScan and ZooProcess (Gorsky et al., 2010), sorted in 127 taxonomic and morphological groups. The ZooCAM dataset is composed of 702,111 zooplankton individuals, zooplankton parts, non-living particles and imaging artefacts individually imaged and measured with the ZooCAM (Colas et al., 2018), sorted in 127 taxonomic and morphological or life stages groups. The total number of different groups identified with both instruments combined is 170, among which 84 are in common (Table 1), 43 belong to the ZooScan dataset only and 43 others belong to the ZooCAM dataset only (Table 2). The identified groups were divided into actual taxa and Operational Taxonomic Units (OTUs). Typically, OTUs are either non-adult life stages of taxa, aggregated morphological groups, or non-living groups (see Tables 1 and 2). Among the groups common to both instruments, 45 are actual taxa, and 39 are OTUs (Table 1). Among the ZooScan only groups, 22 are taxa, and 21 are OTUs, and among the ZooCAM only groups, 18 are taxa, and 25 are OTUs (Table 2).

The differences in identified groups, in the ratio taxa/OTUs, and in the associated counts arose from several aspects of the data generation. Firstly, the two imaging methods differ in their technical set-up. The main difference is that, on the one hand, fixed organisms are laid down and arranged manually on the imaging sensor and digitized in a lab, steady 2-D, set-up when using the ZooScan. On the other hand, organisms are imaged live, in a moving fluid, in a 3-D environment (the flowcell), on-board when digitized with the ZooCAM. Their position in front of the camera may not enable an identification as precise as when they are laid on the scanner tray (Grandremy et al., under review; Colas et al., 2018). Secondly, the dataset are sequential in time, the ZooCAM dataset follows the ZooScan's. Zooplankton communities in the Bay of Biscay may have changed over time, even if their biomass as aggregated groups show a remarkable space-time stability (Grandremy et al., 2023a). Thirdly, we cannot guaranty that there is no adverse effect on taxonomic identification, as validation involved several experts (Culverhouse, 2007). Although we paid great attention to homogenize the final detailed datasets, we recommend to aggregate taxa and OTUs and reduce the biological resolution for ecological studies (Grandremy et al., 2023a, under review). Additionally, numerous identified and sorted taxa and OTUs do not belong to the metazoan zooplankton, or are non-adult life stages, or parts of organisms. Those were included in the presented datasets because they are always found in natural samples. They need to be separated from entire organisms to ensure as accurate as possible abundances estimations, as well as taken into account to ensure accurate biovolumes or biomasses estimations. A good example is the siphonophore issue: numerous swimming bells of degraded siphonophores individuals can be found and imaged in a sample. Determining an accurate siphonophore abundance may not be easy, but this could be overcome by considering the biovolume or biomass of siphonophores by adding up the numerous parts' biovolumes or biomass of the organisms imaged.

252   Table 1: ZooScan and ZooCAM common taxa and OTU. Taxa are listed in the left column of the table, in italics;

253   OTU are listed in the right column of the table in non-italics. OTUs names are spelled as they appear in the dataset.

254   Numbers next to each taxa and OTU are the counts for each category for each instrument in the whole datasets.

255   Non-zooplanktonic OTUs are highlighted in bold.

taxa	ZooCAM counts	ZooScan counts	OTU	ZooCAM counts	ZooScan counts
Acartiidae	30403	66353	**artefact**	**2643**	**60718**
Actinopterygii	85	2113	Bivalvia<Mollusca	1324	3766
Aetideidae	15	75	bract<Diphyidae	1315	386
Amphipoda	68	853	**bubble**	**32563**	**1112**
Annelida	256	2434	calyptopsis<Euphausiacea	1396	3246
Appendicularia	6724	34027	Cnidaria<Metazoa	148	4974
Branchiostoma	15	210	Ctenophora<Metazoa	94	126
Calanidae	9578	91513	cyphonaute	684	2218
Calanoida	137536	149956	cypris	862	2363
Calocalanus	820	1196	dead<Copepoda	13383	17151
Candaciidae	70	2773	**detritus**	**105751**	**219541**
Centropagidae	4592	14651	**Diatoma**	**36842**	**1084**
Chaetognatha	624	7274	**egg sac<egg**	**152**	**394**
Cladocera	5590	18213	**egg unkn temp<Engraulidae temp**	**61**	**192**
Corycaeidae	2021	4720	**egg<Actinopterygii**	**768**	**3596**
Cumacea	4	180	**egg<other**	**17**	**2281**
Decapoda	173	471	eudoxie<Diphyidae	501	69
Doliolida	26	128	**fiber<detritus**	**13379**	**25124**
Echinodermata	24	253	gonophore<Diphyidae	4395	1462
Eucalanidae	2	839	larvae<Annelida	244	708
Euchaetidae	2643	12957	larvae<Echinodermata	483	2200
Euphausiacea	889	1195	larvae<Porcellanidae	127	2838
Euterpina	1043	2870	megalopa	6	460
Foraminifera	1	384	multiple<Copepoda	3740	961
Haloptilus	1	5	multiple<other	1928	10303
Harpacticoida	481	1697	nauplii<Cirripedia	6766	6008
Heterorhabdidae	8	205	nauplii<Crustacea	3422	10747
Insecta	2	3	nectophore<Diphyidae	839	14389
Isopoda	1	123	nectophore<Physonectae	106	696
Limacinidae	8966	6423	**Noctiluca<Noctilucaceae**	**22165**	**20784**
Metridinidae	2333	15081	other<living	15029	5861
Microsetella	116	1169	part<Ctenophora	30	319
Mysida	3	885	part<Siphonophorae	279	12976
Neoceratium	2984	4830	pluteus<Echinodermata	1623	1441
Obelia	459	1016	**scale**	**2**	**53**
Oithonidae	112977	110510	siphonula	1	20
Oncaeidae	11843	34651	tail<Appendicularia	753	11349
Ostracoda	55	341	tomaria larvae	21	83
Phoronida	90	163	zoea<Decapoda	151	1405
Pontellidae	6	299			
Rhincalanidae	1	127			
Sapphirinidae	1	21			
Temoridae	13520	31335			
Thecosomata	15	59			
Tomopteridae	58	618			

256

Table 2: ZooScan and ZooCAM not common taxa and OTU. Taxa and OTUs appearing exclusively in the ZooCAM dataset are listed in the left column, those appearing exclusively in the ZooScan dataset are listed in the right column. For both instruments, taxa are written in italics and OTUs are listed below them in non-italics. OTUs names are spelled as they appear in the dataset. Numbers next to each taxa and OTU are the counts for each category for each instrument in the whole datasets. Non-zooplanktonic taxa and OTUs are highlighted in bold.

taxa/OTU	counts	taxa/OTU	counts
Calocalanus tenuis	17	*Actiniaria*	13
Calycophorae	30	*Aglaura*	1113
Centropages hamatus	8	*Atlanta*	43
Chaetoceros sp.	**9**	*Cavoliniidae*	21
Diphyidae	144	*Cephalopoda*	3
Evadne	1889	*Creseidae*	7
Halosphaera	**193**	*Cymbulia peroni*	3
Hydrozoa	1674	*Euchirella*	239
Isias	51	*Eumalacostraca*	9815
Jaxea	2	*Fritillariidae*	3635
Podon	162	*Harosa*	374
Poecilostomatoida	1094	*Liriope tetraphylla*	121
Pyrosoma	1	*Lubbockia*	1
Rhizaria	**13347**	*Monstrilloida*	1
Sphaeronectidae	4	*Nannosquillidae*	2
Thalassionema	4	*Nemertea*	31
Thaliacea	7	*Paguridae*	4
Trichodesmium	**265**	*Peltidiidae*	133
Aggregata	**253**	*Penaeoidea*	7
chainlarge	**114**	*Pleuromamma*	695
Copepoda X	6727	*Salpida*	470
dead<Harpacticoida	528	*Solmundella bitentaculata*	178
egg 1 temp<Engraulidae temp	**65**	actinula<Hydrozoa	49
egg 1 temp<Sardina temp	**100**	**badfocus<artefact**	**34507**
egg 2 3 temp<Engraulidae temp	**3**	badfocus<Copepoda	11656
egg 2 3 temp<Sardina temp	**49**	ephyra<Scyphozoa	64
egg 4 6 temp<Engraulidae temp	**6**	larvae<Crustacea	114
egg 4 6 temp<Sardina temp	**15**	larvae<Mysida	73
egg 7 8 temp<Engraulidae temp	**13**	larvae<Squillidae	4
egg 9 11 temp<Engraulidae temp	**14**	like<Laomediidae	36
egg 9 11 temp<Sardina temp	**26**	part<Annelida	121
egg unkn temp<Sardina temp	**23**	part<Cnidaria	692
Enteropneusta<Hemichordata	12	part<Crustacea	7530
feces	**227**	part<Thaliacea	44
fluffy<detritus	**3589**	pilidium<Nemertea	12
gelatinous	348	phyllosoma	8
head<Crustacea	9	pluteus<Ophiuroidea	640
larvae<Ascidiacea	1	protozoea<Mysida	229
larvae<Gastropoda	116	protozoea<Penaeidae	28
light<detritus	**38126**	protozoea<Sergestidae	12
Rhizaria X	**857**	tail<Chaetognatha	251
Rhizosolenids	**761**	trunk<Appendicularia	1210
veliger	113	zoea<Galatheidae	660

263   OTUs' names are mainly in the form of two words separated by a "<" character. Although we tried to name them

264   as most explicitly as possible, a few potentially needed clarifications can be found in Table 3.

265   Table 3: Non-exhaustive list of prefixes, their types (morphological, developmental stage, taxonomical, non-living

266   and imaging artefact), and content.

prefix	type	content of category
bract	morphological	single siphonophore bracts
eudoxie	morphological	single siphonophore Eudoxia zooids
gonophore	morphological	single siphonophore gonozooids
nectophore	morphological	single siphonophore swimming bells
trunk	morphological	single appendicularian trunks detached from their tails
tail	morphological	appendicularian's or chaethognath's tail shaped part of the body
head	morphological	individual organisms' heads detached from the body
part	morphological	unidentified body part
egg sac	morphological	detached copepod egg sacs
like	morphological	look alike, without absolute certainty
multiple	morphological	two or more objects touching each other in the same vignette
other	morphological	non-identified living object
actinula	developmental stage	undefined hydrozoa actinula larval stage
calyptopsis	developmental stage	Euphausiacea calyptopsis larval stage
egg	developmental stage	egg larval stage
ephira	developmental stage	ephira hydrozoa larval stage
larvae	developmental stage	undefined larval stage
nauplii	developmental stage	crustacean nauplius larval stage
pilidium	developmental stage	free-swimming larva of nemertean worm
protozoea	developmental stage	crustacean protozoea larval stage
pluteus	developmental stage	Echinodermata pluteus larval stage
zoea	developmental stage	crustacean zoea larval stage
egg 1 temp	developmental stage	clupeid fish embryo developemental stage 1*
egg 2 3 temp	developmental stage	clupeid fish embryo developemental stages 2 and 3 aggregated*
egg 4 6 temp	developmental stage	clupeid fish embryo developemental stages 4 to 6 aggregated*
egg 7 8 temp	developmental stage	clupeid fish embryo developemental stages 7 and 8 aggregated*
egg 9 11 temp	developmental stage	clupeid fish embryo developemental stages 9 to 11 aggregated*
egg unknown	developmental stage	clupeid fish unidentified embryo developemental stage*
Bivalvia	taxonomical	small bivalve larvae of unidenfified mollusca
dead	non_living	copepod's exuvia, carcass or part of dead body
fiber	non_living	fiber like detritus
fluffy	non_living	vey porous detritic particles
light	non_living	very transparent detritic particles
badfocus	imaging artefact	out-of-focus objects

267

268   * clupeids fish embryo developmental stages according to Ahlstrom (1943) and Moser & Ahlstrom (1985).

269
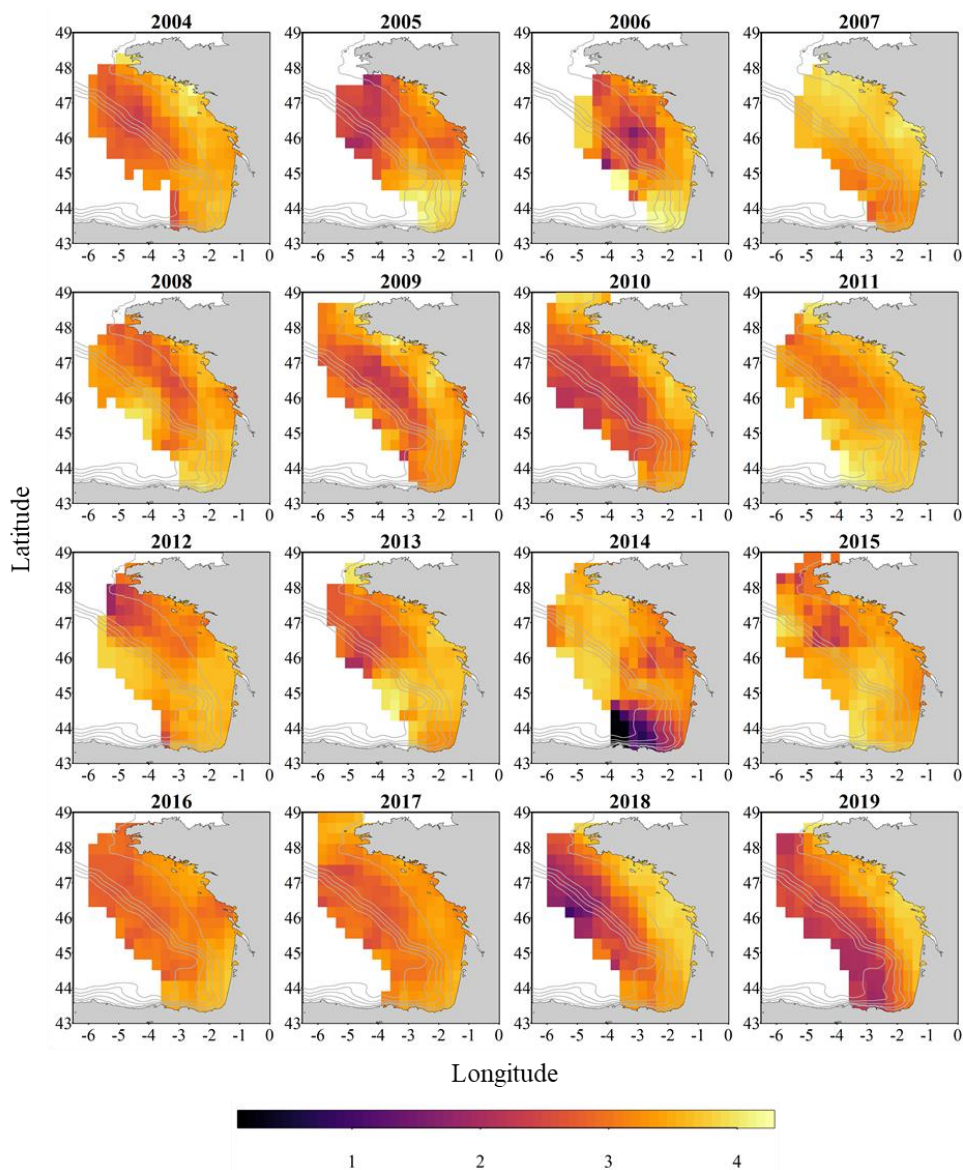
Figure 4: Gridded maps of total zooplankton Shannon index (calculated on spherical biovolumes) during the
PELGAS cruise in the Bay of Biscay from 2004 to 2019. Shannon index exhibit a coastal to offshore gradient as
well as a north-south gradient. Shannon index is larger at the coast and in the south, except in 2014 where it is
smaller in the south, offshore.

274 **3.2 Data and images**

275 **3.2.1 Data**

276   The data is divided into two datasets available as tab separated files, one for each instrument. Within each

277 dataset the data is organized as a table containing text data as well as numerical data. Each dataset combines

278 together actual data and metadata at the individual object granularity. For each object, the user will be able to find

279 descriptors originating from the image processing (i.e. features), and sampling metadata (i.e. latitude and longitude

280 of sampling station, date and time of sampling, sampling device, etc.) and sample processing metadata (i.e.

281 subsampling factor, seawater sampled volume, pixel size), in columns, and individual objects in lines. The columns

282 headers are defined in Tables A1 and A2 for ZooCAM and ZooScan datasets respectively. The following prefixes

283 enable the segregation of types of data and metadata: (i) "object_", which identifies variables assigned to each

284 object individually; (ii) "sample_", which identifies variables assigned to each sample; (iii) "acq_", which

285 identifies variables assigned to each data acquisition for the same sample (note here that this type of variable is

286 found only in the ZooScan dataset as ZooScan samples were splitted in two size fractions corresponding to two

287 acquisitions); (iv) "process_", which identifies variables describing key image processing features (i.e. pixel size).

288 Those prefixes originate from the use of the Ecotaxa web application to sort and identify the images (Picheral et

289 al., 2017) that promote this specific formatting. The ZooCAM dataset is shaped as a 72 columns (variables) x

290 702,111 rows (individual imaged objects) matrix and the ZooScan dataset is shaped as a 71 columns (variables) x

291 1,153,507 rows (individual imaged objects) matrix.

292 Among the 70+ variables it is worth noticing the following ones:

293 (i)   objid: it is a unique individual object numerical identifier that enables to link single data line to a
294   corresponding single image in the image dataset;

295 (ii)   taxon: it is the taxonomic or OTU identification of the imaged objects written as they appear in the
296   Tables 1 and 2;

297 (iii) lineage: it is the full taxonomic lineage of the taxon. Lineage may be used to aggregate taxa at a higher
298   taxonomic levels, respecting taxonomic lineages;

299 (iv)   classif_id: it is a unique, numerical, taxon identifier;

300 (v)   sample_sub_part / acq_sub_part: those are the subsampling ratios, for ZooCAM and ZooScan
301   respectively, needed to reconstruct the quantitative estimates of the samples' abundances;

302 (vi)   sample_fishingvolume / sample_tot_vol: those are the total seawater sampled volumes for ZooCAM
303   and ZooScan respectively, needed to normalize the samples' concentrations by seawater volume.

304 One can therefore calculate quantitative abundances estimates for a taxon in a sample as follow:

305 ZooCAM: $Ab_{taxon} = \frac{n_{taxon} \times sample\_sub\_part}{sample\_fishingvolume}$ (1)

306 ZooScan: $Ab_{taxon} = \frac{\left(n_{taxon_{acq1}} \times acq\_sub\_part_{acq1}\right) + \left(n_{taxon_{acq2}} \times acq\_sub\_part_{acq2}\right)}{sample\_tot\_vol}$ (2)

307 Where Ab is the abundance in $ind.m^{-3}$ and n is the number of individuals for "taxon".

3.2.2 Images

Two sets of individual images sorted into folders by categories (Tables 1 and 2) come along with each dataset. For the ZooCAM only, the associated images from years 2016 and 2017 contain printed Region Of Interest (ROI) bounding box limits and text at the bottom of each image, and non-homogenised background within and around the ROI bounding box; images from year 2018 contain non-homogenised background within the ROI bounding box only; images from 2019 have a completely homogeneous and thresholded background around the object. The differences arose from successive ZooCAM software updates that do not modify the calculation of object's features. The ZooScan images have all a completely homogeneous and thresholded background around the object, no bounding box limits nor text printed in the images. All images for the two instruments datasets have a 1 mm scale bar printed at the bottom left corner.

4 Data availability

The ZooScan dataset can be found as the ***PELGAS Bay of Biscay ZooScan zooplankton Dataset (2004-2016)*** in the SEANOE dataportal following the link: https://www.seanoe.org/data/00829/94052/ (Grandremy et al., 2023b). The ZooCAM dataset can be found as the ***PELGAS Bay of Biscay ZooCAM zooplankton Dataset (2016-2019)*** in the SEANOE dataportal https://www.seanoe.org/data/00828/94040/ (Grandremy et al., 2023c).

Each dataset comes as a .zip archive that contains:

- One tab separated file containing all data and metadata associated to each imaged and identified object.
- One comma separated file containing the name, type, definition and unit of each field (column)
- One comma separated file containing the taxonomic list of the dataset, with counts and nature of the content of the category
- A directory "*individual_images*" containing images of each object, named according to the object id *objid* and sorted in subdirectories according to their taxonomic identification, across years and sampling stations.

5 Concluding remarks

Recent studies showed that the small pelagic fish (SPF) communities have suffered from a drastic decrease of condition in the Mediterranean Sea and in the Bay of Biscay (Van Beveren et al., 2014; Doray et al., 2018b; Saraux et al., 2019) over the last 20 years. This loss of condition was especially expressed by the constant decrease of SPF size- and weight-at-age (Doray et al., 2018b; Veron et al. 2020), and possibly explained by a change in SPF trophic resource composition, size and quality (Brosset et al., 2016; Queiros et al., 2019; Menu et al., 2023). Identifying and measuring zooplankton at appropriate temporal and spatial scales is not an easy task, but can be addressed with imaging. These datasets were assembled as an effort to make possible the exploration of the relationship between SPF observed dynamics in the Bay of Biscay and their main food resource's dynamics, the metazoan zooplankton. This zooplankton imaging data series is a significant output of Nina Grandremy PhD (2019-2023), that is currently being exploited (Grandremy et al., 2023a), and is intended to be continued and updated on a yearly basis in the framework of the PELGAS program, to better understand the underlying processes presiding to long-term SPF dynamics. Moreover, those two zooplankton datasets can be associated with the PELGAS survey datasets previously published in 2018, also in the SEANOE dataportal, featuring hydrological, primary producers, fish and megafauna data arranged as gridded data (Doray et al., 2018a). Together, all these

346   datasets allow to study simultaneously all the pelagic ecosystem compartments, with coherent spatial domain (the
347   Bay of Biscay continental shelf), resolution and time series. Nevertheless, a spatial gridding of the data is highly
348   recommended (as represented in the Fig. 2, 3 and 4), since the spatial coverage of the sampling protocols can vary
349   between years (Fig. 1), within and between each pelagic ecosystem compartment. A procedure for such batch data
350   spatial smoothing is presented e.g. in Petitgas et al. (2009, 2014). See also Doray et al. (2018b) and Grandremy et
351   al. (2023a) for application examples. As several descriptors of the spring zooplankton community (abundances,
352   sizes, biovolumes, biomass) can be derived from this 16 years long spatially resolved time series at several
353   taxonomic levels, these datasets are intended to be used in various ecological studies including the zooplankton
354   compartment, especially modelling studies, where zooplankton is usually underrepresented (Mitra, 2010; Mitra et
355   al., 2014). Finally, these datasets can also be used for machine learning applied to plankton studies serving, for
356   example, as consequent learning sets.

357   **Disclaimer**

358   Data are published without any warranty, express or implied. The user assumes all risk arising from his/her use of
359   data. Data are intended to be research-quality, but it is possible that the data themselves contain errors. It is the
360   sole responsibility of the user to assess if the data are appropriate for his/her use, and to interpret the data
361   accordingly. Authors welcome users to ask questions and report problems.

362   **Authors' contributions**

363   GN scanned and validated most of the ZooScan dataset, assembled the datasets, and led the drafting. BP collected
364   and managed the samples since 2004, and participated in the manual validation of identifications. DE scanned a
365   substantial fraction of the ZooScan samples and participated in the initial sorting of vignettes. DMM participated
366   in the collection of samples, and was involved in the ZooCAM development. DM was chief scientist on the
367   PELGAS surveys and participated in the drafting. DC supervised GN work and participated in the drafting. FB
368   developed, improved and maintained the ZooCAM software. JL curated a substantial fraction of the ZooScan
369   dataset manual validation of identifications. HM participated in the collection of samples, lead the DEFIPEL
370   project, and participated in the drafting. LMS participated in the collection of samples, and managed the ZooCAM.
371   NA curated a substantial fraction of the ZooScan and ZooCAM dataset manual validation of identifications. PP
372   supervised GN work and participated in the drafting. PPh participated in the collection of samples and participated
373   in the drafting. RJ supervised the development and improvement of the ZooCAM. TM developed and improved
374   the ZooCAM, and participated in the collection of samples. RJB supervised GN work, participated in the collection
375   of samples, curated a substantial fraction of the ZooCAM dataset manual validation of identifications, and lead
376   the drafting.

377   **Competing interests**

378   The authors declare that they have no conflict of interest.

379   **Acknowledgements**

380   The authors acknowledge receiving funding from the 'France Filière Pêche' DEFIPEL project. NG acknowledges
381   the funding of her PhD by Region Pays de la Loire, FR and Ifremer. The authors wish to thank Jean-Yves Coail,
382   Gérard Guyader and Patrick Berriet (Ifremer – REM-RDT-SIIM) for their contribution to the hardware assembly
383   of the ZooCAM. The authors acknowledge the work of Elio Raphalen for scanning year 2005 samples. The authors

thank the EMBRC platform PIQs for image analysis. This work was supported by EMBRC-France, whose French state funds are managed by the ANR within the Investments of the Future program under reference ANR-10-INBS-02. Finally, the authors wish also to thank the many other students, technicians and scientists who participated in the sampling and samples imaging on board, and the successive crews of the R/V *Thalassa* involved in the PELGAS surveys from 2004 to 2019.

References

Ahlstrom, E.H., 1943. Studies on the Pacific Pilchard Or Sardine (Sardinops Caerulea): Influence of Temperature on the Rate of Development of Pilchard Eggs in Nature. United States Department of the Interior, Fish and Wildlife Service.

Banse, K., 1995. Zooplankton: Pivotal role in the control of ocean production: I. Biomass and production. ICES Journal of Marine Science 52, 265–277. https://doi.org/10.1016/1054-3139(95)80043-3

Batten, S.D., Abu-Alhaija, R., Chiba, S., Edwards, M., Graham, G., Jyothibabu, R., Kitchener, J.A., Koubbi, P., McQuatters-Gollop, A., Muxagata, E., Ostle, C., Richardson, A.J., Robinson, K.V., Takahashi, K.T., Verheye, H.M., Wilson, W., 2019. A Global Plankton Diversity Monitoring Program. Frontiers in Marine Science 6.

Beaugrand, G., Brander, K.M., Lindley, J.A., Souissi, S., Reid, P.C., 2003. Plankton effect on cod recruitment in the North Sea. Nature 426, 661–664. https://doi.org/10.1038/nature02164

Benedetti, F., Jalabert, L., Sourisseau, M., Becker, B., Cailliau, C., Desnos, C., Elineau, A., Irisson, J.-O., Lombard, F., Picheral, M., Stemmann, L., Pouline, P., 2019. The Seasonal and Inter-Annual Fluctuations of Plankton Abundance and Community Structure in a North Atlantic Marine Protected Area. Front. Mar. Sci. 6. https://doi.org/10.3389/fmars.2019.00214

Breiman, L., 2001. Random forests. Mach. Learn. 45, 5–32. https://doi.org/10.1023/A:1010933404324

Brosset, P., Le Bourg, B., Costalago, D., Banaru, D., Van Beveren, E., Bourdeix, J.-H., Fromentin, J.-M., Menard, F., Saraux, C., 2016. Linking small pelagic dietary shifts with ecosystem changes in the Gulf of Lions. Mar. Ecol.-Prog. Ser. 554, 157–171. https://doi.org/10.3354/meps11796

Chiba, S., Batten, S., Martin, C.S., Ivory, S., Miloslavich, P., Weatherdon, L.V., 2018. Zooplankton monitoring to contribute towards addressing global biodiversity conservation challenges. Journal of Plankton Research 40, 509–518. https://doi.org/10.1093/plankt/fby030

Colas, F., Tardivel, M., Perchoc, J., Lunven, M., Forest, B., Guyader, G., Danielou, M.M., Le Mestre, S., Bourriau, P., Antajan, E., Sourisseau, M., Huret, M., Petitgas, P., Romagnan, J.B., 2018. The ZooCAM, a new in-flow imaging system for fast onboard counting, sizing and classification of fish eggs and metazooplankton. Progress in Oceanography, Multidisciplinary integrated surveys 166, 54–65. https://doi.org/10.1016/j.pocean.2017.10.014

Culverhouse, P.F., 2007. Human and machine factors in algae monitoring performance. Ecol. Inform. 2, 361–366. https://doi.org/10.1016/j.ecoinf.2007.07.001

418 Cury, P., Bakun, A., Crawford, R.J.M., Jarre, A., Quiñones, R.A., Shannon, L.J., Verheye, H.M., 2000. Small
419 pelagics in upwelling systems: patterns of interaction and structural changes in "wasp-waist" ecosystems. ICES
420 Journal of Marine Science 57, 603–618. https://doi.org/10.1006/jmsc.2000.0712

421 Doray, M., Huret, M., Authier, M., Duhamel, E., Romagnan, J.-B., Dupuy, C., Spitz, J., Sanchez, F., Berger, L.,
422 Dorémus, G., Bourriau, P., Grellier, P., Pennors, L., Masse, J., Petitgas, P., 2018a. Gridded maps of pelagic
423 ecosystem parameters collected in the Bay of Biscay during the PELGAS integrated survey.
424 https://doi.org/10.17882/53389

425 Doray, M., Petitgas, P., Huret, M., Duhamel, E., Romagnan, J.B., Authier, M., Dupuy, C., Spitz, J., 2018b.
426 Monitoring small pelagic fish in the Bay of Biscay ecosystem, using indicators from an integrated survey. Progress
427 in Oceanography 166, 168–188. https://doi.org/10.1016/j.pocean.2017.12.004

428 Doray, M., Petitgas, P., Romagnan, J.B., Huret, M., Duhamel, E., Dupuy, C., Spitz, J., Authier, M., Sanchez, F.,
429 Berger, L., Dorémus, G., Bourriau, P., Grellier, P., Massé, J., 2017. The PELGAS survey: Ship-based integrated
430 monitoring of the Bay of Biscay pelagic ecosystem. Progress in Oceanography.
431 https://doi.org/10.1016/j.pocean.2017.09.015

432 Elineau, A., Desnos, C., Jalabert, L., Olivier, M., Romagnan, J.-B., Costa Brandao, M., Lombard, F., Llopis, N.,
433 Courboulès, J., Caray-Counil, L., Serranito, B., Irisson, J.-O., Picheral, M., Gorsky, G., Stemmann, L., 2018.
434 ZooScanNet: plankton images captured with the ZooScan. https://doi.org/10.17882/55741

435 Feuilloley, G., Fromentin, J.-M., Saraux, C., Irisson, J.-O., Jalabert, L., Stemmann, L., 2022. Temporal fluctuations
436 in zooplankton size, abundance, and taxonomic composition since 1995 in the North Western Mediterranean Sea.
437 ICES J. Mar. Sci. 79, 882–900. https://doi.org/10.1093/icesjms/fsab190

438 Gorsky, G., Ohman, M.D., Picheral, M., Gasparini, S., Stemmann, L., Romagnan, J.-B., Cawood, A., Pesant, S.,
439 Garcia-Comas, C., Prejger, F., 2010. Digital zooplankton image analysis using the ZooScan integrated system. J.
440 Plankton Res. 32, 285–303. https://doi.org/10.1093/plankt/fbp124

441 Graham, B., 2014. Spatially-sparse convolutional neural networks. https://doi.org/10.48550/arXiv.1409.6070

442 Grandremy, N., Romagnan, J.-B., Dupuy, C., Doray, M., Huret, M., Petitgas, P., 2023a. Hydrology and small
443 pelagic fish drive the spatio–temporal dynamics of springtime zooplankton assemblages over the Bay of Biscay
444 continental shelf. Progress in Oceanography 210, 102949. https://doi.org/10.1016/j.pocean.2022.102949

445 Grandremy N., Bourriau P., Daché E., Danielou M-M., Doray M., Dupuy C., Huret M., Jalabert L., Le Mestre S.,
446 Nowaczyk A., Petitgas P., Pineau P., Raphalen E., Romagnan J-B., 2023b. PELGAS Bay of Biscay ZooScan
447 zooplankton Dataset (2004-2016). SEANOE. https://doi.org/10.17882/94052

448 Grandremy N., Bourriau P., Danielou M-M., Doray M., Dupuy C., Forest B., Huret M., Le Mestre S., Nowaczyk
449 A., Petitgas P., Pineau P., Rouxel J., Tardivel M., Romagnan J-B., 2023c. PELGAS Bay of Biscay ZooCAM
450 zooplankton Dataset (2016-2019). SEANOE. https://doi.org/10.17882/94040

451 Grandremy N., Dupuy C., Petitgas P., Le Mestre S., Bourriau P., Nowaczyk A., Forest B., Romagnan J-B. The
452 ZooScan and the ZooCAM zooplankton imaging systems are intercomparable: A benchmark on the Bay of Biscay
453 zooplankton. *Limnology and Oceanography: Methods*. Under review.

454 Ho,   J.S.,   2001.   Why   do   symbiotic   copepods   matter?   Hydrobiologia   453,   1–7.
455 https://doi.org/10.1023/A:1013139212227

456 ICES, 2021. Bay of Biscay and Iberian Coast ecoregion – Fisheries overview (report). ICES Advice: Fisheries
457 Overviews. https://doi.org/10.17895/ices.advice.9100

458 Irisson, J.-O., Ayata, S.-D., Lindsay, D.J., Karp-Boss, L., Stemmann, L., 2022. Machine Learning for the Study of
459 Plankton   and   Marine   Snow   from   Images.   Annual   Review   of   Marine   Science   14,   277–301.
460 https://doi.org/10.1146/annurev-marine-041921-013023

461 Lombard, F., Boss, E., Waite, A.M., Vogt, M., Uitz, J., Stemmann, L., Sosik, H.M., Schulz, J., Romagnan, J.-B.,
462 Picheral, M., Pearlman, J., Ohman, M.D., Niehoff, B., Möller, K.O., Miloslavich, P., Lara-Lpez, A., Kudela, R.,
463 Lopes, R.M., Kiko, R., Karp-Boss, L., Jaffe, J.S., Iversen, M.H., Irisson, J.-O., Fennel, K., Hauss, H., Guidi, L.,
464 Gorsky, G., Giering, S.L.C., Gaube, P., Gallager, S., Dubelaar, G., Cowen, R.K., Carlotti, F., Briseño-Avena, C.,
465 Berline, L., Benoit-Bird, K., Bax, N., Batten, S., Ayata, S.D., Artigas, L.F., Appeltans, W., 2019. Globally
466 Consistent   Quantitative   Observations   of   Planktonic   Ecosystems.   Front.   Mar.   Sci.   6.
467 https://doi.org/10.3389/fmars.2019.00196

468 Menu, C., Pecquerie, L., Bacher, C., Doray, M., Hattab, T., van der Kooij, J., Huret, M., 2023. Testing the bottom-
469 up hypothesis for the decline in size of anchovy and sardine across European waters through a bioenergetic
470 modeling approach. Progress in Oceanography 210, 102943. https://doi.org/10.1016/j.pocean.2022.102943

471 Mitra, A., Castellani, C., Gentleman, W.C., Jonasdottir, S.H., Flynn, K.J., Bode, A., Halsband, C., Kuhn, P.,
472 Licandro, P., Agersted, M.D., Calbet, A., Lindeque, P.K., Koppelmann, R., Moller, E.F., Gislason, A., Nielsen,
473 T.G., John, M.S., 2014. Bridging the gap between marine biogeochemical and fisheries sciences; configuring the
474 zooplankton link. Prog. Oceanogr. 129, 176–199. https://doi.org/10.1016/j.pocean.2014.04.025

475 Mitra, A., Davis, C., 2010. Defining the "to" in end-to-end models. Prog. Oceanogr. 84, 39–42.
476 https://doi.org/10.1016/j.pocean.2009.09.004

477 Moser, H.G., Ahlstrom, E.H., 1985. Staging anchovy eggs. Southwest Fisheries Center, National Marine Fisheries
478 Service, NOM, PO. Box 271, La Jolla, CA 92038.

479 Ohman, M.D., Romagnan, J.-B., 2016. Nonlinear effects of body size and optical attenuation on Diel Vertical
480 Migration by zooplankton. Limnology and Oceanography 61, 765–770. https://doi.org/10.1002/lno.10251

481 Orenstein, E.C., Ayata, S.-D., Maps, F., Becker, É.C., Benedetti, F., Biard, T., de Garidel-Thoron, T., Ellen, J.S.,
482 Ferrario, F., Giering, S.L.C., Guy-Haim, T., Hoebeke, L., Iversen, M.H., Kiørboe, T., Lalonde, J.-F., Lana, A.,
483 Laviale, M., Lombard, F., Lorimer, T., Martini, S., Meyer, A., Möller, K.O., Niehoff, B., Ohman, M.D., Pradalier,
484 C., Romagnan, J.-B., Schröder, S.-M., Sonnet, V., Sosik, H.M., Stemmann, L.S., Stock, M., Terbiyik-Kurt, T.,
485 Valcárcel-Pérez, N., Vilgrain, L., Wacquet, G., Waite, A.M., Irisson, J.-O., 2022. Machine learning techniques to

486 characterize functional traits of plankton from image data. Limnology and Oceanography 67, 1647–1669.

487 https://doi.org/10.1002/lno.12101

488 Panaïotis, T., Caray–Counil, L., Woodward, B., Schmid, M.S., Daprano, D., Tsai, S.T., Sullivan, C.M., Cowen,

489 R.K., Irisson, J.-O., 2022. Content-Aware Segmentation of Objects Spanning a Large Size Range: Application to

490 Plankton Images. Frontiers in Marine Science 9.

491 Petitgas, P., Goarant, A., Masse, J., and Bourriau, P., 2009. Combining acoustic and CUFES data for the quality

492 control of fish-stock survey estimates. ICES Journal of Marine Science, 66: 1384–1390.

493 https://doi.org/10.1093/icesjms/fsp007

494 Petitgas, P., Doray, M., Huret, M., Masse´, J., and Woillez, M., 2014. Modelling the variability in fish spatial

495 distributions over time with empirical orthogonal functions: anchovy in the Bay of Biscay. ICES Journal of Marine

496 Science, 71: 2379–2389. https://doi.org/10.1093/icesjms/fsu111

497 Queiros, Q., Fromentin, J.-M., Gasset, E., Dutto, G., Huiban, C., Metral, L., Leclerc, L., Schull, Q., McKenzie,

498 D.J., Saraux, C., 2019. Food in the Sea: Size Also Matters for Pelagic Fish. Frontiers in Marine Science 6.

499 https://doi.org/10.3389/fmars.2019.00385

500 Romagnan, J.B., Aldamman, L., Gasparini, S., Nival, P., Aubert, A., Jamet, J.L., Stemmann, L., 2016. High

501 frequency mesozooplankton monitoring: Can imaging systems and automated sample analysis help us describe

502 and interpret changes in zooplankton community composition and size structure - An example from a coastal site.

503 Journal of Marine Systems 162, 18–28. https://doi.org/10.1016/j.jmarsys.2016.03.013

504 Saraux, C., Beveren, E.V., Brosset, P., Queiros, Q., Bourdeix, J.-H., Dutto, G., Gasset, E., Jac, C., Bonhommeau,

505 S., Fromentin, J.-M., 2019. Small pelagic fish dynamics: A review of mechanisms in the Gulf of Lions. Deep Sea

506 Research Part II: Topical Studies in Oceanography 159, 52–61. https://doi.org/10.1016/j.dsr2.2018.02.010

507 Sieburth, J., Smetacek, V., Lenz, J., 1978. Pelagic Ecosystem Structure - Heterotrophic Compartments of Plankton

508 and Their Relationship to Plankton Size Fractions - Comment. Limnol. Oceanogr. 23, 1256–1263.

509 https://doi.org/10.4319/lo.1978.23.6.1256

510 Siegel, D.A., Buesseler, K.O., Behrenfeld, M.J., Benitez-Nelson, C.R., Boss, E., Brzezinski, M.A., Burd, A.,

511 Carlson, C.A., D'Asaro, E.A., Doney, S.C., Perry, M.J., Stanley, R.H.R., Steinberg, D.K., 2016. Prediction of the

512 Export and Fate of Global Ocean Net Primary Production: The EXPORTS Science Plan. Frontiers in Marine

513 Science 3.

514 Steinberg, D.K., Carlson, C.A., Bates, N.R., Goldthwait, S.A., Madin, L.P., Michaels, A.F., 2000. Zooplankton

515 vertical migration and the active transport of dissolved organic and inorganic carbon in the Sargasso Sea. Deep

516 Sea Research Part I: Oceanographic Research Papers 47, 137–158. https://doi.org/10.1016/S0967-0637(99)00052-

517 7

518 Turner, J.T., 2015. Zooplankton fecal pellets, marine snow, phytodetritus and the ocean's biological pump.

519 Progress in Oceanography 130, 205–248. https://doi.org/10.1016/j.pocean.2014.08.005

520   Uitz, J., Claustre, H., Gentili, B., Stramski, D., 2010. Phytoplankton class-specific primary production in the
521   world's oceans: Seasonal and interannual variability from satellite observations. Global Biogeochemical Cycles
522   24.

523   Van Beveren, E., Bonhommeau, S., Fromentin, J.-M., Bigot, J.-L., Bourdeix, J.-H., Brosset, P., Roos, D., Saraux,
524   C., 2014. Rapid changes in growth, condition, size and age of small pelagic fish in the Mediterranean. Mar Biol
525   161, 1809–1822. https://doi.org/10.1007/s00227-014-2463-1

526   Vandromme, P., Nogueira, E., Huret, M., Lopez-Urrutia, A., Gonzalez-Nuevo Gonzalez, G., Sourisseau, M.,
527   Petitgas, P., 2014. Springtime zooplankton size structure over the continental shelf of the Bay of Biscay. Ocean
528   Sci. 10, 821–835. https://doi.org/10.5194/os-10-821-2014

529   Vandromme, P., Stemmann, L., Garcìa-Comas, C., Berline, L., Sun, X., Gorsky, G., 2012. Assessing biases in
530   computing size spectra of automatically classified zooplankton from imaging systems: A case study with the
531   ZooScan integrated system. Methods in Oceanography 1–2, 3–21. https://doi.org/10.1016/j.mio.2012.06.001

532   Véron, M., Duhamel, E., Bertignac, M., Pawlowski, L., Huret, M., 2020. Major changes in sardine growth and
533   body condition in the Bay of Biscay between 2003 and 2016: Temporal trends and drivers. Progress in
534   Oceanography 182, 102274. https://doi.org/10.1016/j.pocean.2020.102274

535

536 **Appendix A**

537 Table A1: ZooCAM dataset columns header – definition of data and metadata fields.

column name	definition
object_id	name of object and associated image
objid	unique ecotaxa internal object identifier
object_lat	latitude of sampling
object_lon	longitude of sampling
object_date	date of sampling
object_time	time of sampling
object_depth_min	minimum sampling depth
object_depth_max	maximum sampling depth
object_taxon	taxonomic name
object_lineage	full taxonomic lineage corresponding to the taxon
classif_id	unique ecotaxa internal taxon identifier
object_area	object's surface
object_area_exc	object surface excluding white pixels
object_%area	proportion of the image corresponding to the object
object_area_based_diameter	object's Area Based Diameter: 2 * (object_area/pi)^(1/2)
object_meangreyimage	mean image grey level
object_meangreyobjet	mean object grey level
object_modegreyobjet	modal object grey level
object_sigmagrey	object grey level standard deviation
object_mingrey	minimum object grey level
object_maxgrey	maximum object grey level
object_sumgrey	object grey level integrated density: object_mean*object_area
object_breadth	breadth of the object along the best fitting ellipsoid minor axis
object_length	breadth of the object along the best fitting ellipsoid majorr axis
object_elongation	elongation index: object_length/object_breadth
object_perim	object's perimeter
object_minferetdiam	minimum object's feret diameter
object_maxferetdiam	maximum object's feret diameter
object_meanferetdiam	average object's feret diameter
object_feretelongation	elongation index: object_maxferetdiam/object_minferetdiam
object_compactness	Isoperimetric quotient: the ratio of the object's area to the area of a circle having the same perimeter
object_intercept0	number of times that a transition from background to foreground occurs a the angle 0° for the entire object
object_intercept45	the number of times that a transition from background to foreground occurs a the angle 45° for the entire object
object_intercept90	the number of times that a transition from background to foreground occurs a the angle 90° for the entire object
object_intercept135	the number of times that a transition from background to foreground occurs a the angle 135° for the entire object
object_convexhullarea	area of the convex hull of the object
object_convexhullfillratio	ratio object_area/convexhullarea
object_convexperimeter	perimeter of the convex hull of the object
object_n_number_of_runs	number of horizontal strings of consecutive foreground pixels in the object
object_n_chained_pixels	number of chained pixels in the object
object_n_convex_hull_points	number of summits of the object's convex hull polygon
object_n_number_of_holes	number of holes (as closed white pixel area) in the object
object_transparence	ratio object_sumgrey/obejct_area
object_roughness	measure of small scale variations of amplitude in the object's grey levels
object_rectangularity	ratio of the object's area over its best bounding rectangle's area
object_skewness	skewness of the object's grey level distribution
object_kurtosis	kurtosis of the object's grey level distribution
object_fractal_box	fractal dimension of the object's perimeter
object_hist25	grey level value at quantile 0.25 of the object's grey levels normalized cumulative histogram
object_hist50	grey level value at quantile 0.5 of the object's grey levels normalized cumulative histogram
object_hist75	grey level value at quantils 0.75 of the object's grey levels normalized cumulative histogram
object_valhist25	sum of grey levels at quantile 0.25 of the object's grey levels normalized cumulative histogram
object_valhist50	sum of grey levels at quantile 0.5 of the object's grey levels normalized cumulative histogram
object_valhist75	sum of grey levels at quantile 0.75 of the object's grey levels normalized cumulative histogram
object_nobj25	number of objects after thresholding at the object_valhist25 grey level
object_nobj50	number of objects after thresholding at the object_valhist50 grey level
object_nobj75	number of objects after thresholding at the object_valhist75 grey level
object_symetrieh	index of horizontal symmetry
object_symetriev	index of vertical symmetry
object_thick_r	maximum object's thickness/mean object's thickness
object_cdist	distance between the mass and the grey level object's centroids
object_bord	tag for object touching the frame edge
sample_id	name of the sample from where the object originates
sample_ship	name of the ship used to collect the samples
sample_campaign	name of the cruise where samples were collected
sample_station	name of the station where samples were collected
sample_depth	bottom depth at station
sample_device	net used to collect the sample
sample_fishingvolume	seawater volume sampled
sample_sub_part	subsampling elevation factor
process_id	name of software/software version used to analysed digitized sample images
process_resolution_camera_micron	pixel size, μm

538

539   Table A2: ZooScan dataset columns header – definition of data and metadata fields

column name	definition
object_id	name of object and associated image
objid	unique ecotaxa internal object identifier
object_lat	latitude of sampling
object_lon	longitude of sampling
object_date	date of sampling
object_time	time of sampling
object_depth_min	minimum sampling depth
object_depth_max	maximum sampling depth
object_taxon	taxonomic name
object_lineage	full taxonomic lineage corresponding to the taxon
classif_id	unique ecotaxa internal taxon identifier
object_area	object's surface
object_mean	mean object grey level
object_stddev	object grey level standard deviation
object_mode	modal object grey level
object_min	minimum object grey level
object_max	maximum object grey level
object_perim.	object's perimeter
object_major	lenght of major axis of best fitting elipse
object_minor	lenght of minor axis of best fitting elipse
object_circ.	circularity: 4*pi(object_area/object_perim.^2)
object_feret	maximum feret diameter
object_intden	object grey level integrated density : /object_mean*/object_area
object_median	median object grey level
object_skew	skewness of the object's grey level distribution
object_kurt	kurtosis of the object's grey level distribution
object_%area	proportion of the image corresponding to the object
object_area_exc	object surface excluding white pixels
object_fractal	fractal dimension of the object's perimeter
object_skelarea	surface of the one-pixel wide skeleton of the object
object_slope	slope of the cumulated histogram of the object grey levels
object_histcum1	the number of times that a transition from background to foreground occurs at the angle0°
object_histcum2	grey level at quantiles 0.5 of the histogram of the object grey levels
object_histcum3	grey level at quantiles 0.75 of the histogram of the object grey levels
object_nb1	number of objects after thresholding at the object_histcum1 grey level
object_nb2	number of objects after thresholding at the object_histcum2 grey level
object_symetrieh	index of horizontal symmetry
object_symetriev	index of vertical symmetry
object_symetriehc	index of horizontal symmetry after thresholding at the object_histcum1 grey level
object_symetrievc	index of vertical symmetry after thresholding at the object_histcum1 grey level
object_convperim	perimeter of the convex hull of the object
object_convarea	area of the convex hull of the object
object_fcons	object's contrast
object_thickr	maximum object's thickness/mean object's thickness
object_esd	object's Equivalent Spherical Diameter: 2 * (object_area/pi)^(1/2)
object_elongation	elongation index: major/minor
object_range	range of greys: max-min
object_meanpos	relative position of the mean grey: (max-mean)/range
object_centroids	distance between the mass and the grey level object's centroids
object_cv	coefficient of variation of greys: 100*(stddev/mean)
object_sr	index of variation of greys: 100*(stddev/range)
object_perimareaexc	index of the relative complexity of the perimeter: object_perim/object_area_exc
object_feretareaexc	another elongation index : object_feret/object_area_exc
object_perimferet	index of the relative complexity of the perimeter: object_perim/object_feret
object_perimmajor	index of the relative complexity of the perimeter: object_perim/object_major
object_circex	circularity of object excluding white pixels: 4*pi(object_area_exc/object_perim.^2)
object_cdexc	distance between the mass and the grey level object's centroids calculated with object_area_exc
sample_id	name of the sample from the object originate
sample_ship	name of the ship used to collect the samples
sample_program	name of the cruise where samples were collected
sample_stationid	name of the station where samples were collected
sample_bottomdepth	bottom depth at station
sample_net_type	net used to collect the sample
sample_tot_vol	seawater volume sampled
sample_comment	comments associated with sampling/sample treatment
process_id	name of software/software version used to analysed digitized sample images
process_particle_pixel_size_mm	pixel size
acq_id	name of subsample if any
acq_min_mesh	minimum sieve size of subsample
acq_max_mesh	maximum sieve size of subsample
acq_sub_part	subsampling elevation factor

540

541